Apatites and britholites, are they akin - as probed by Eu^{3+} luminescence?

2001 J. Phys.: Condens. Matter 13 537

(http://iopscience.iop.org/0953-8984/13/3/313)

INSTITUTE OF PHYSICS PUBLISHING JOURNAL OF PHYSICS: CONDENSED MATTER

J. Phys.: Condens. Matter **13** (2001) 537–547 www.iop.org/Journals/cm PII: S0953-8984(01)14303-1

Apatites and britholites, are they akin—as probed by Eu^{3+} luminescence?

K Marimuthu[1], L C Nehru[2], A Mani[2], R Ramesh[2], G Muralidharan[1] and R Jagannathan[2,3]

[1] Gandhigram Rural Institute, Gandhigram-624302 (TN), India
[2] Luminescence Group, CECRI, Karaikudi-630006 (TN), India

E-mail: jags57_99@yahoo.com (R Jagannathan)

Received 30 May 2000, in final form 12 September 2000

Abstract

Britholite, a relatively little known cousin of the celebrated apatites, has been prepared by solid-state reaction methods. In samples of hexagonal $Y_{6-x}Ca_4(SiO_4)_6F_2{:}Eu^{3+}_x$ ($x = 0.5$–4%) britholite prepared by using Eu^{3+} luminescence as a local probe, we found that there are two kinds of cationic site, in the same way as for the apatites. But these two sites appear to have nearly the same local symmetry, which is considerably different from the case for the fluoro-apatite counterpart.

1. Introduction

Apatites, pyromorphites and britholites are some of the oxygen-dominated matrices showing dimorphism and these can be crystallized under hexagonal ($P6_3/m$) and monoclinic ($P2_1$) systems. These materials, in particular the apatites, find a variety of applications ranging from conventional to very advanced ones. For example, fluorescent lighting and biocompatible ceramics are well known fields where apatites are widely used [1, 2]. Apatites already find extensive application [3, 4] while the britholites are relatively new, and information on the structural aspects appears to be limited [5]. Interestingly, the rare-earth-containing britholites seem to have major application in nuclear waste storage and for this reason this system has been studied extensively, for example, by Boyer *et al* [6, 7]. In order to determine the suitability of these materials for several applications, knowledge of the structural aspects is essential. Especially as regards predicting interesting optical properties, information concerning the local site symmetry of the cationic site(s) is very important, and it will be helpful in proposing new applications. Hence we thought it worthwhile to compare these systems and elicit more information concerning the cationic site symmetry(ies). For this purpose we employed Eu^{3+} luminescence, the well known structural probe. In this context it is relevant to mention that the results of our earlier work using Eu^{3+} luminescence as a spectral probe in various apatites [8] are consistent with similar work by other research groups [9, 10].

[3] Author to whom any correspondence should be addressed.

Although apatites are of various types, ranging from conventional halo-apatites to oxy-apatites formed by arsenate, vanadate or chromate groups [11, 12], the former is more popular as far as applications are concerned. Here, in this investigation as a specific case, we compare the results on Eu^{3+} luminescence in calcium fluoro-apatite ($Ca_{10-x}(PO_4)_6F_2{:}Eu_x^{3+}$; $x = 0.5$–4%) and in a britholite constituted from yttrium calcium fluorosilicate/silico-phosphate ($Y_{6-x}Ca_4(SiO_4)_6F_2{:}Eu_x^{3+}$ where $x = 0.5$–4%; in the case of silico-phosphate the composition was $Y_{6-x}Ca_4(SiO_4)_3(PO_4)_3F_2{:}Eu_x^{3+}$). We consider that these two can serve well as representative examples of the apatite and britholite systems, to allow us to achieve some insight into the structural similarities. Hence a broad generalization should become possible, with the luminescence data as the basis.

2. Experimental procedure

All of the starting materials used were analysed reagents.

The Ca fluoro-apatite sample with Eu^{3+} used in this investigation was the same as that described earlier [8]. For the preparation of Eu^{3+}-doped britholite, the reactants taken in proportion were consistent with equation (1):

$$3CaCO_3 + 3[(1 - x/6)Y_2O_3 + (x/6)(Eu_2O_3)] + 6SiO_2 + CaF_2 \rightarrow Ca_4Y_{6-x}(SiO_4)_6F_2{:}Eu_x + 3CO_2\uparrow \quad (1)$$

($x = 0.5$ to 4% wrt Ca^{2+}) and were homogenized using an agate mortar. For the preparation of phospho-silicate-based britholites, a proportion of the silicate was replaced by phosphate using di-ammonium hydrogen orthophosphate (DAP).

Then the mixture was calcined at 1200 °C for 30 h with intermittent homogenization. In the preparation of the britholites, special attention was paid to ensuring the completion of the reaction. In particular, if the heating was incomplete, in the fluorescence spectrum a characteristic emission of $Y_2O_3{:}Eu^{3+}$ at 612 nm corresponding to the $^5D_0 \rightarrow {}^7F_2$ transition appeared. Hence the firing was continued (intermittently) until the $Y_2O_3{:}Eu^{3+}$ emission peak disappeared. Finally the product, a white mass, was gently crushed and used for the characterization and further studies. The chemical purity of the product was checked with the help of an x-ray powder diffractometer (employing Cu Kα radiation) as described before [8]. The diffraction patterns obtained in these cases were consistent with $P6_3/m$ (apatite) or $P2_1$ (britholite) space-group symmetries and the crystallographic cell parameters listed in table 1 were obtained by following a standard least-squares fitting procedure. In the case of britholite,

Table 1. Least-squares refined crystallographic cell parameters for $Y_{6-x}Ca_4(SiO_4)_6F_2{:}Eu_x^{3+}$ britholite compared with the Ca fluoro-apatite system.

		Crystallographic cell parameters					
System	Space-group symmetry	a (Å)	b (Å)	c (Å)	α (deg)	β (deg)	γ (deg)
Ca fluoro-apatite (JCPDS standard)	$P6_3/m$	9.4240	9.4240	6.8880	90.00	90.00	120.00
Ca fluoro-apatite	$P6_3/m$	9.4513	9.4513	6.9149	90.00	90.00	120.00
Y britholite (standard)*	$P2_1$	9.3620	9.3640	6.7310	89.99	90.02	120.00
YCa britholite	As $P2_1$	9.4205	9.4127	6.7609	90.00	91.00	90.00
YCa britholite	As $P6_3$	9.3620	9.3640	6.7310	90.00	90.00	120.00

* Reference [5].

as the structural information on this system is limited, the XRD data were indexed under both hexagonal and monoclinic systems.

The photoluminescence (PL) studies on these samples were made in the same way as described earlier [8]. It should be mentioned that in the case of the britholite system the x-ray diffraction patterns as well as the fluorescence spectra for both the YCa fluorosilicate ($Y_{6-x}Ca_4(SiO_4)_6F_2{:}Eu_x^{3+}$) type of britholite and the phosphate-substituted YCa fluorosilicate ($Y_{6-x}Ca_4(SiO_4)_3(PO_4)_3F_2{:}Eu_x^{3+}$) type of britholite are found to be identical. This implies that in the britholite system, the replacement of silicate $(SiO_4)^{2-}$ by phosphate $(PO_4)^{3-}$ does not introduce any structural changes.

3. Results and discussion

3.1. Macroscopic symmetry of apatites and britholites

The crystallography of apatites is well documented in the literature [13] while the related information on the britholite analogue appears to be limited. However, these systems have identical structural features, as implied from the similar space-group symmetries, be it a hexagonal $P6_3/m$ ($P6_3$) or a monoclinic $P2_1$ symmetry. In general, the britholite resembles apatite in atomic arrangement in spite of the fact that the former is constituted by a large number of lanthanide and other ions having different sizes. Then main difference between the apatite and britholite structures is that the apatite system constituted by rigid $(PO_4)^{3-}$ tetrahedra gives little scope for any distortion while the britholite is made of a less rigid $(SiO_4)^{2-}$ network undergoing considerable readjustment in the Si–O bond lengths. There are differences in the cation (Ca^{2+}/Ln^{3+})–O^{2-} bond length(s) between successive metal-ion–oxygen triangles along the c-direction (z-axis). This difference in the bond lengths can lower the crystal symmetry of the britholite in two ways:

(i) absence of a mirror plane perpendicular (symmetry element $/m$) to the c-axis with the lattice symmetry lowered to $P6_3$;
(ii) complete removal of the $3/m$ symmetry element with the lattice symmetry lowered to monoclinic $P2_1$.

This hexagonal-to-monoclinic distortion observed in the britholite leads to a minor change in the crystallographic cell parameters. This is reflected in the emergence of additional lines in the XRD pattern (figure 1) of the britholite sample which are consistent with the absence of extinction conditions for $0kl$, $l = 2n$ and for $h0l$, $l = 2n$. The difference in symmetry elements available between the apatite and britholite can be represented pictorially with the help of figures 2(a) and 2(b). Apart from this information, there is little crystallographic information available on the britholites constituted by various lanthanide, transition metal and alkaline-earth ions of disparate sizes. In the present investigation we deal with a pure britholite YCa silicate system corresponding to the formula $Ca_4Y_6(SiO_4)_6F_2$ (or with at the most a few per cent of Eu^{3+} substituted for yttrium). In view of the limited crystallographic information on britholites, we attempted to refine the x-ray diffraction data obtained under both the hexagonal and the monoclinic symmetries by using a least-squares refinement procedure. The fitted values, under both symmetries, are given in table 1 and from this it is obvious that for the britholite system the agreement is better under a monoclinic $P2_1$ symmetry than under a hexagonal $P6_3/m$ setting. Further, from figure 1, it is obvious that the diffraction patterns of the britholite samples corresponding to YCa silicate and YCa silico-phosphate are identical. This implies isostructural substitution of phosphate for silicates in the britholite system. Also, it has been found that the fluorescence spectra are identical in the two cases. For these reasons,

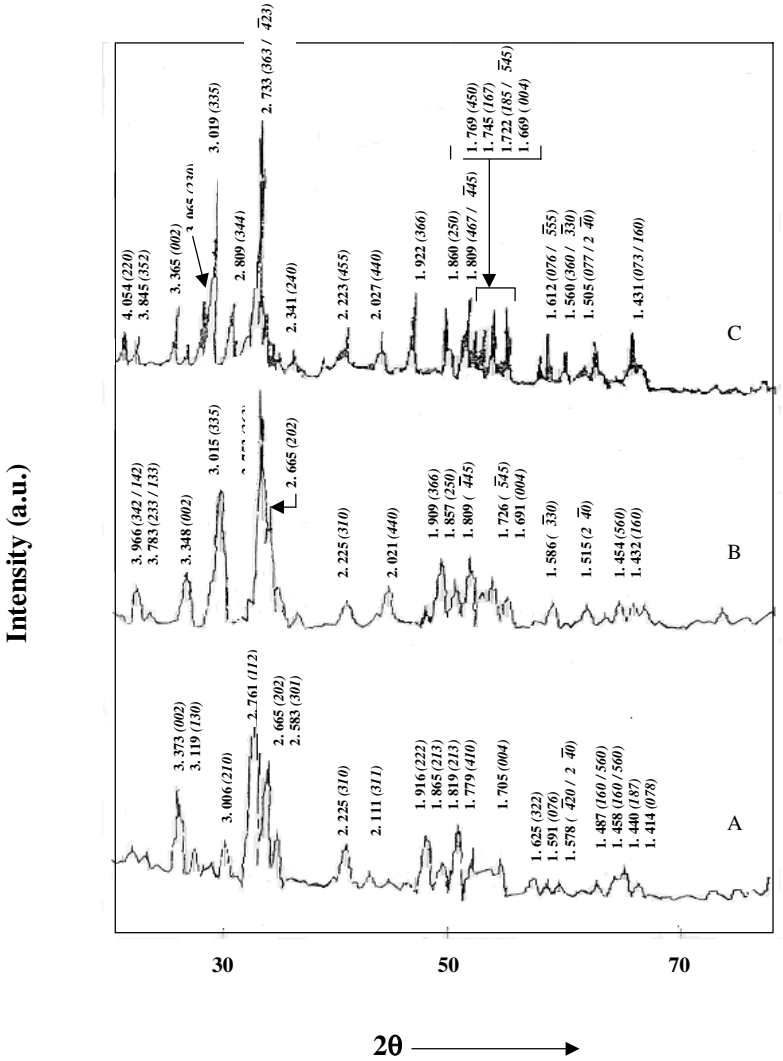

Figure 1. Comparison of XRD patterns (Cu Kα radiation at $T = 300$ K) of YCa britholite and Ca fluoro-apatite consistent with $P6_3/m$ and $P2_1$ space-group symmetries.

we discuss only the results corresponding to the YCa silicate system, which for all practical purposes can be assumed to represent the britholite system.

3.2. Cationic site(s) in apatites and britholites

Eu^{3+} can serve as a successful local probe for eliciting information concerning the multiplicity of the cationic sites and their symmetries in several host matrices [14, 15]. This is possible with

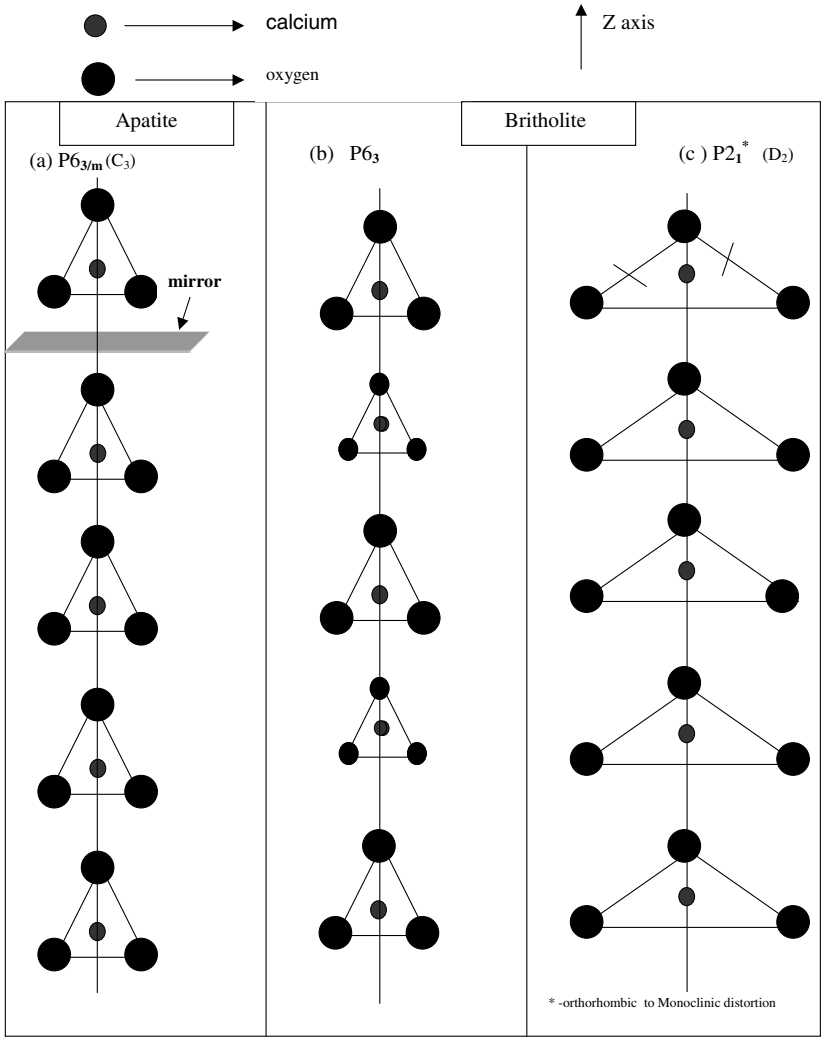

Figure 2. Comparison of lattice (and local) symmetries in apatite and britholite.

the knowledge of the Stark-splitting pattern: the occurrence of the non-degenerate ($^5D_0 \rightarrow {}^7F_0$) and the hypersensitive ($^5D_0 \rightarrow {}^7F_2$) transitions of Eu^{3+}. The conclusions derived using this technique will be more reliable, especially when Eu^{3+} occupies host matrices without requiring charge-compensating species (that is, when occupying sites of trivalent host cations). This is because charge-compensating species or the defects produced arising out of aliovalent substitution may distort the site symmetry. Since the Stark-splitting pattern carries information on the site symmetry, it is essential that a reasonable degree of spectral resolution is maintained while recording the luminescence spectrum.

Before describing the results of the present investigation, we consider that a brief mention of the different types of excitation to be employed would be appropriate. Excitation near the absorption edge of the host matrix or in the Eu^{3+}–O^{2-} charge-transfer band, usually around 260 nm, will be characteristic of the host matrix and hence this can be called *selective excitation*. On the other hand, excitation in the Eu^{3+} levels in particular, where the oscillator strength of the

transition is high—for example, excitation around 395 nm corresponding to the $^7F_0 \rightarrow {}^5D_2$ transition of Eu^{3+}—constitutes a *non-selective* excitation. Hence in the case of the former excitation, we can observe emission only from a selected type of Eu^{3+} site(s) appropriate for the excitation, while in the case of the latter, Eu^{3+} emission from different kinds of site can be observed.

On inspection of the emission and excitation spectra given in figures 3 and 4, we see two sets of signals (marked I and II) in the britholite:Eu^{3+} system, implying the presence of two kinds of cationic site. Basically, the luminescence yield of Eu^{3+} in britholite does not seem to be as efficient as that observed in the case of the apatite system. This makes clear analysis of the emission spectrum difficult. Notwithstanding this shortcoming however, we focus our

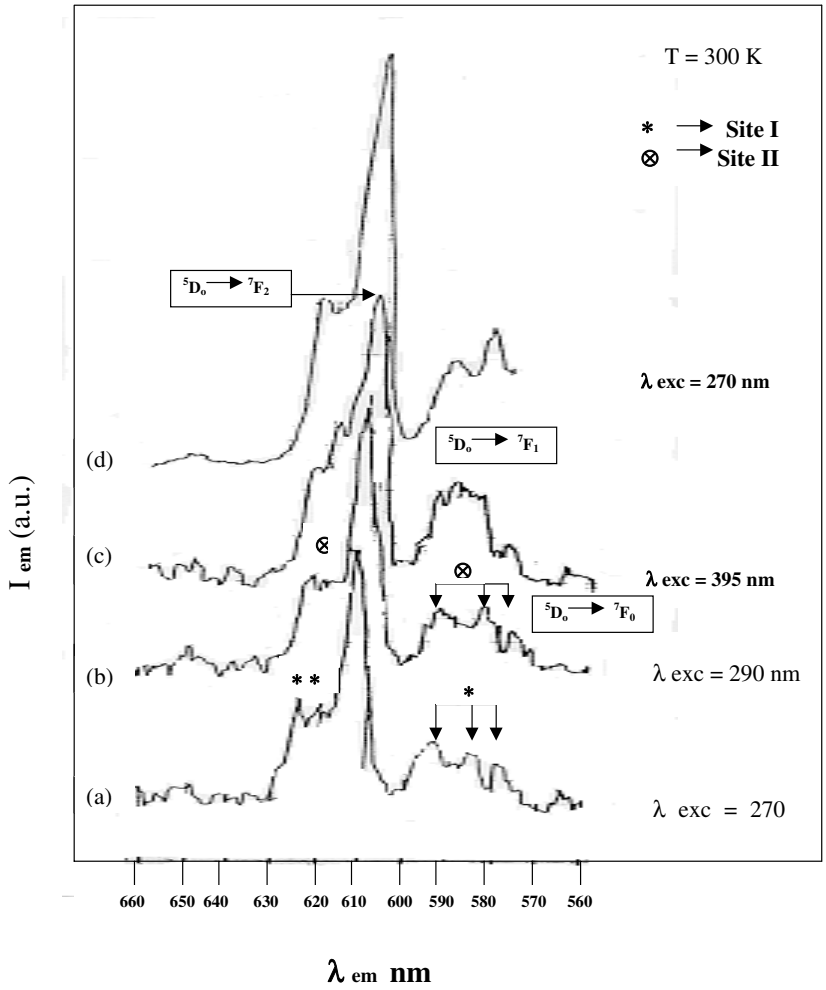

Figure 3. The emission spectrum of Eu^{3+} (4%) in britholite (silicate) ($Ca_4Y_{6-x}(SiO_4)_6F_2$:Eu^{3+}_x) under various excitations: (a) selective excitation (Eu^{3+}–O^{2-} charge-transfer band; $\lambda_{exc} = 270$ nm) corresponding to one kind of Eu^{3+} site; (b) selective excitation (Eu^{3+}–O^{2-} charge-transfer band; $\lambda_{exc} = 290$ nm) corresponding to another kind of Eu^{3+} site; (c) non-selective excitation ($^7F_0 \rightarrow {}^5D_2$) of Eu^{3+} at $\lambda_{exc} = 395$ nm; and (d) Eu^{3+} (4%) in britholite (silico-phosphate) ($Ca_4Y_{6-x}(SiO_4)_3(PO_4)_3F_2$:$Eu^{3+}_x$).

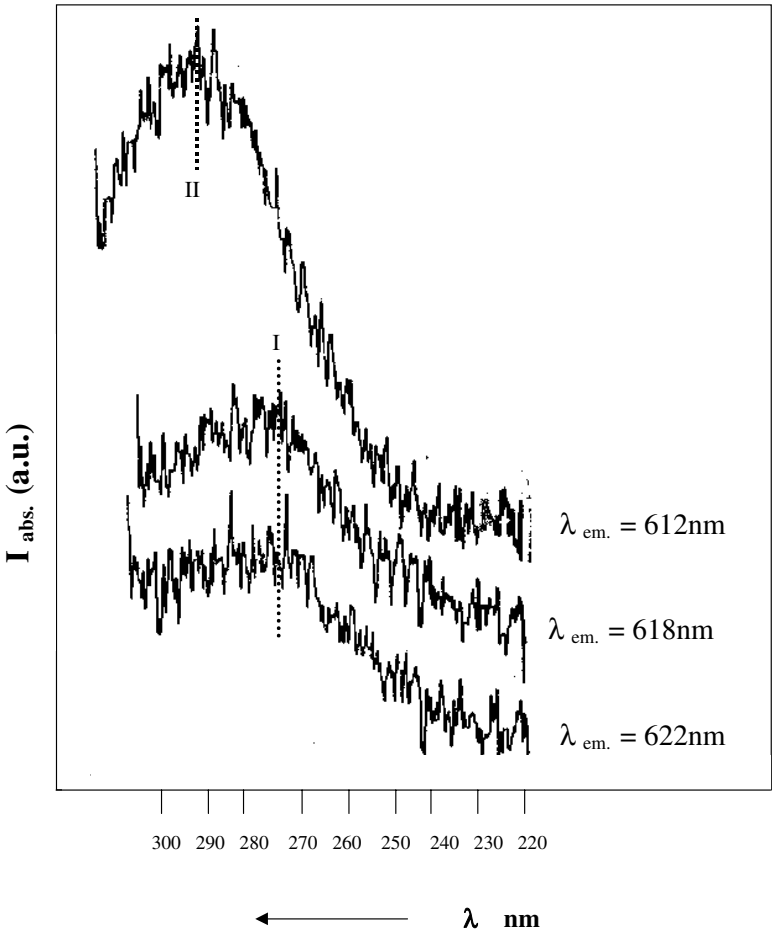

Figure 4. The excitation spectrum of Eu^{3+} (4%) in YCa britholite monitoring different emission components of the dominant $^5D_0 \rightarrow {}^7F_2$ emission (at $\lambda_{em} = 612$, 618 and 622 nm).

attention on the hypersensitive $^5D_0 \rightarrow {}^7F_2$ transition (showing moderate intensity), which can serve well the purpose of a structural probe. For the case of non-selective excitation, two sets of signals appear for the $^5D_0 \rightarrow {}^7F_2$ transition. Obviously, the excitation spectra monitoring 618 and 622 nm Stark components lead to identical excitation patterns, maximized at 275 nm, while that corresponding to the 612 nm component leads to an excitation maximum of 290 nm (figure 4). Here we would like to stress that the latter component cannot be attributed to Y_2O_3:Eu^{3+} emission (as an impurity phase due to the starting material, by virtue of the lack of chemical purity of the sample prepared), because the excitation maximum in this case lies at much shorter wavelengths (∼230 nm) [16]. Further, it is important to mention that the 612 nm component is broader than the other two components and is skewed (marked by a bold arrow) to the longer-wavelength side. This implies the presence of an additional Stark component in this set of signals. Further, it is significant that, unlike that for Ca fluoro-apatite:Eu^{3+} [8], in the case of Eu^{3+} emission in britholite, it is independent of the Eu^{3+} concentration. This implies the absence of a concentration-dependent site occupancy mechanism in the britholite system. Hence for all practical purposes we can assume that there are five Stark components in each set

of signals (corresponding to 270 and 290 nm selective excitations in figure 3) corresponding to the hypersensitive transition (table 2). As for the $^5D_0 \rightarrow {}^7F_1$ magnetic dipole transition, we can see two sets of emission lines each containing three weak components in the region of 580 to 600 nm. Further, as for the non-degenerate $^5D_0 \rightarrow {}^7F_0$ emission, there are two weak signals in the region of 570 to 580 nm, one each for the cases of selective excitation at 270 and 290 nm. Hence it is obvious that we can conclude that there are at least two kinds of cationic site occupied by Eu^{3+} in the britholite system. A possible Stark-splitting pattern for the various $^5D_0 \rightarrow {}^7F_J$ ($J = 0$–2) transitions is given in table 2.

Table 2. Comparison of spectroscopic data on Eu^{3+} luminescence in apatite and britholite. IIR $\equiv I(^5D_0 \rightarrow {}^7F_0)/I(^5D_0 \rightarrow {}^7F_1)$. BDR $\equiv 4B_{20}^2/375\Delta_{20}^2$.

		$^5D_0 \rightarrow {}^7F_J$ and Stark components (cm^{-1})							
System	Site	$J = 0$	$J = 1$	$J = 2$	B_{20} (cm^{-1})	Δ_{20} (cm^{-1})	BDR	IIR	Comments
Britholite	M_I	17241 (A_1)	17094 16835 16778 ($A_2 + B_1 + B_2$)	16366 16286 16181 16090 16000 ($2A_1 + A_2 + B_1 + B_2$)	316	993.6	0.001	0.1363	D_2 symmetry
	M_{II}	17301 (A_1)	17094 16835 16778 ($A_2 + B_1 + B_2$)	16339 16260 16155 16129 16051 ($2A_1 + A_2 + B_1 + B_2$)	259	1119.3	0.0005	0.1818	D_2 symmetry
Calcium fluoro-apatite	M_{II}	17361 (A)	17212 17123 16995 (A + E)	16515 16247 16048 16012 (A + 2B + E)	362	949.9	0.001	1.5	C_4 symmetry (modified)
	M_I	17483 (A)	17050 16935 16828 ($A + E_1$)	16083 15987 15936 ($A + E_1 + E_2$)		1481			C_3 symmetry

3.3. The non-degenerate $^5D_0 \rightarrow {}^7F_0$ emission and the cationic site symmetry

In order to assign the site symmetry for the various cationic sites occupied by Eu^{3+}, we have to consider different possibilities. In the britholite system under investigation, there are two types of cation, namely Ca^{2+} and Y^{3+}. In the case of Ca fluoro-apatite, the unique cation Ca^{2+} occurs in two types of configuration, namely at a nine-coordinated site (with oxygen) showing C_3 symmetry and at a seven-coordinated site (with six oxygens and one fluoride) showing C_{1h} symmetry [13]. The Ca^{2+} sites in the fluoro-apatite system when occupied by Eu^{3+} (as a luminescent species) seem to undergo considerable modification, probably dictated by the

charge-compensating defects resulting from the aliovalent substitution of Eu^{3+} for Ca^{2+}. This suggests a symmetry higher than that predicted by the crystallographic studies [8]. Now we compare the results based on Eu^{3+} luminescence in the apatite and the britholite systems: we believe that the case of the latter (notwithstanding the isomorphism exhibited by the two) is slightly different in the sense that the presence of Eu^{3+} at a trivalent Y^{3+} site does not require charge-compensating species. Further, there can be at least two distinct cationic sites due to Ca^{2+} and Y^{3+}. Apart from this marked difference in the Stark-splitting pattern (figure 5), suggesting a difference in local symmetry between the two systems, there is another important difference, namely the absence of intense $^5D_0 \rightarrow {}^7F_0$ emission in the britholite system. From figure 5 and table 2 it can be seen that the same $^5D_0 \rightarrow {}^7F_0$ emission is very intense in the fluoro-apatite (with an intensity ratio of about 1.5 with respect to the structure-independent $^5D_0 \rightarrow {}^7F_1$ transition). This again suggests a major difference in site symmetry between the two systems.

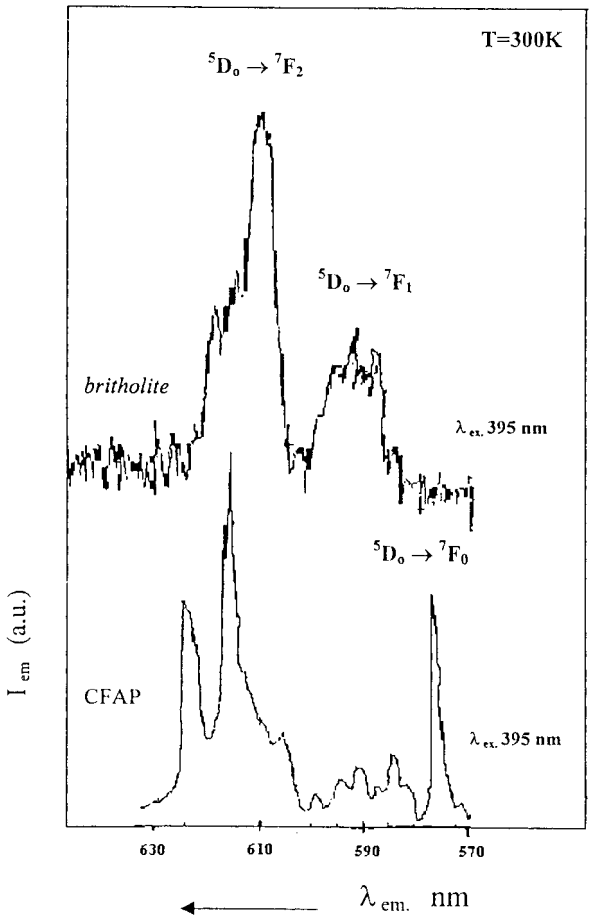

Figure 5. Comparison of the fluorescence spectra of Eu^{3+} (4%) in YCa britholite and Ca fluoro-apatite, to illustrate the absence of intense $^5D_0 \rightarrow {}^7F_0$ emission in the former.

The occurrence of intense $^5D_0 \rightarrow {}^7F_0$ emission, the otherwise forbidden (both by spin and parity selection rules) non-degenerate transition, can be explained on the basis of either of the following two mechanisms:

(i) intensity borrowing from the hypersensitive $^5D_0 \rightarrow {}^7F_2$ transition by J-mixing effects;
(ii) breakdown of the closure approximation based on the site symmetry (as a result of the inclusion of linear terms in the crystal field).

If the former is the active mechanism, the relative intensity of the $^5D_0 \rightarrow {}^7F_0$ emission with respect to the $^5D_0 \rightarrow {}^7F_2$ emission is a few per cent, and this ratio varies as $4B_{20}^2/375\Delta_{20}^2$ [17]. B_{20} is the second-order crystal-field parameter and Δ_{20} is the energy separation between the $^7F_0$, $^7F_2$ manifolds. B_{20} can be determined with the knowledge of the splitting between the Stark levels of the $^5D_0 \rightarrow {}^7F_1$ transition and this has been determined for the cases of Eu^{3+} in fluoro-apatite and britholite as given in table 2.

On the other hand in the case of the latter mechanism being active, the relative intensity of the forbidden transition will be nearing unity. This type of emission has been observed in other matrices [18]. In order for the latter to be an active mechanism, the closure approximation (the condition ensuring the admixture of odd-parity states) should not be applicable. This will be facilitated by non-centrosymmetric sites having linear terms in the crystal-field potential such as C_s or C_{nv} or C_n symmetries. Alternatively, the presence of a dihedral (D_n symmetry being slightly higher) symmetry element may result in a weak emission intensity for the non-degenerate transition. It is obvious from figure 5 that in the case of the fluoro-apatite the intensity ratio works out to be nearly 1.5 while in the case of the britholite this works out to be about 0.1–0.2. Now the pertinent question is that of whether in the case of the Ca fluoro-apatite the high intensity ratio realized is due to the breakdown of the closure approximation or not. In any case, there seems to be an obvious difference between the mechanisms responsible for the occurrence of the forbidden transition in the two systems. Further, the high intensity for the non-degenerate transition can only be explained by the breakdown of the closure approximation induced by the symmetry-sensitive linear crystal-field terms. It is important to note that for this to happen, the charge-transfer state due to the Eu^{3+} ligand should lie at much lower energy [19]. But in the excitation spectra (figure 4), comparing the positions of the Eu^{3+} ligand (usually O^{2-}) charge-transfer state in the two cases, we observe that for both it is around 290 nm. Hence we consider that in the britholite system the site symmetry prevailing at the cationic sites occupied by Eu^{3+} should have higher symmetry that excludes linear field terms in the expression for the crystal field acting on the Eu^{3+} levels. Further, the moderately intense $^5D_0 \rightarrow {}^7F_2$ emission and a weak $^5D_0 \rightarrow {}^7F_0$ emission observed suggest a non-centrosymmetric site lacking a σ_h reflection plane. Hence these results (including the Stark-splitting pattern for the Eu^{3+} levels) can probably be described with a minimum local symmetry corresponding to the D_2 point-group symmetry. In order for this orthorhombic point group to fit into a monoclinic lattice ($P2_1$ space-group symmetry), it is possible that the britholite system might need to undergo a slight orthorhombic-to-monoclinic distortion (figure 2(c)).

Finally, it is rather surprising that Eu^{3+} emission in britholite (notwithstanding that a significant proportion of the Eu^{3+} ions occupy trivalent Y^{3+} sites) is not as efficient as in Y_2O_3:Eu^{3+} or Ca fluoro-apatite:Eu^{3+}. We believe that this can probably be attributed to the increased non-radiative losses in the excited state(s) owing to the less rigid $(SiO_4)^{4-}$ anionic network of the silicate group.

4. Conclusions

Eu^{3+}-doped britholite-type CaY fluorosilicate shows mild red fluorescence under UV excitation (λ_{exc} = 260–290 nm). The low luminescence yield in the britholite system (as compared to Y_2O_3:Eu^{3+} red phosphor or Ca fluoro-apatite:Eu^{3+}) can be attributed to pronounced non-radiative losses in the excited state(s) due to the less rigid $(SiO_4)^{4-}$ anionic network. Eu^{3+} as

a local probe in this system reveals the presence of at least two kinds of site (that are probably due to Ca^{2+} and Y^{3+} ions) of nearly equal symmetry corresponding to the D_2 point group. This is certainly higher than the local symmetry observed in the fluoro-apatite system. Further, the luminescence results suggest that although the macroscopic symmetries of the britholite and apatite can be related, the microscopic symmetries of the cationic sites are very different.

Acknowledgments

Our sincere thanks to both of the referees of the earlier version of the manuscript for valuable critical comments, and also to the Director, CECRI, for all of the experimental facilities.

References

[1] Butler K H 1986 *Fluorescent Lamp Phosphors* (University Park, PA: Pennsylvania State University Press)
[2] Liu Q, de Wijn J R and van Blitterswjik C A 1997 *Biomaterials* **18** 1253
[3] Yamashita K and Umegaki T 1995 *Inorg. Mater.* **2** 166
[4] Monma H 1982 *J. Catal.* **75** 200
[5] Noe D C, Hughes J M, Mariano A N, Drexler J W and Kato A 1993 *Z. Kristallogr.* **206** 233
[6] Meis C, Gale J D, Boyer L, Carpena J and Gosset D 2000 *J. Phys. Chem.* A **104** 5380
[7] Boyer L, Carpena J and Lacout J L 1996 *Solid State Ion.* **95** 121
[8] Jagannathan R and Kottaisamy M 1995 *J. Phys.: Condens. Matter* **7** 8453
[9] Reisfeld R *et al* 1996 *J. Lumin.* **69** 343
[10] El Ouenzerfi R, Kbir-Ariguib N, Trabelsi-Ayedi M and Piriou B 1999 *J. Lumin.* **85** 71
[11] Jun Lin and Qiang Su 1994 *J. Alloys Compounds* **210** 159
[12] Bemoussa H, Mikon M and Lacout J L 1999 *Mater. Res. Bull.* **34** 1429
[13] Ropp R C 1991 *Luminescence and the Solid State (Studies in Inorganic Chemistry vol 12)* (Amsterdam: Elsevier) ch 10
[14] Nieuwpoort W C, Blasse G and Bril A 1967 *Proc. Johns Hopkins University Conf.* (New York: Interscience) p 161
[15] Blasse G 1975 *J. Solid State Chem.* **14** 181
[16] Justel T, Bechtel H, Nikol H, Ronda C R and Wiechert D U 1998 *Proc. Electrochem. Soc.* **98-24** 103
[17] Nishimura G, Tanaka M, Kurita A and Kushida T 1991 *J. Lumin.* **48+49** 473
[18] Wang Q, Gao Y and Bulou A 1995 *J. Phys. Chem. Solids* **56** 285
[19] Tanaka M, Nishimura G and Kushida T 1994 *Phys. Rev.* B **49** 16 917